Spatiotemporal dynamics of doxorubicin elution from embolic beads within a microfluidic network

Dario Carugo, Lorenzo Capretto, Bibhas Roy, Michele Carboni, Marcus Caine, Andrew L. Lewis, Martyn Hill, Suman Chakraborty, Xunli Zhang

PII: S0168-3659(15)30017-1
DOI: doi: 10.1016/j.jconrel.2015.07.003
Reference: COREL 7750

To appear in: *Journal of Controlled Release*

Received date: 10 March 2015
Revised date: 30 June 2015
Accepted date: 1 July 2015

Please cite this article as: Dario Carugo, Lorenzo Capretto, Bibhas Roy, Michele Carboni, Marcus Caine, Andrew L. Lewis, Martyn Hill, Suman Chakraborty, Xunli Zhang, Spatiotemporal dynamics of doxorubicin elution from embolic beads within a microfluidic network, *Journal of Controlled Release* (2015), doi: 10.1016/j.jconrel.2015.07.003

Spatiotemporal dynamics of doxorubicin elution from embolic beads within a microfluidic network

Dario Carugo[a,e,*,†], *Lorenzo Capretto*[a,†], *Bibhas Roy*[b,†], *Michele Carboni*[a], *Marcus Caine*[a,c,d], *Andrew L Lewis*[c,d], *Martyn Hill*[e,f], *Suman Chakraborty*[g] *and Xunli Zhang* [a,f]

[a] Bioengineering Science Research Group, Faculty of Engineering and the Environment, University of Southampton, Southampton SO17 1BJ, United Kingdom

[b] Department of Biotechnology, Indian Institute of Technology Kharagpur, Kharagpur 721302, India

[c] Biocompatibles UK Ltd., a BTG International group company, Farnham Business Park, Weydon Lane, Farnham, Surrey GU9 8QL, United Kingdom

[d] BTG International Ltd., 5 Fleet Place, London EC4M 7RD, United Kingdom

[e] Electromechanical Research Group, Faculty of Engineering and the Environment, University of Southampton, Southampton SO17 1BJ, United Kingdom

[f] Institute for Life Sciences, University of Southampton, Southampton, SO17 1BJ, United Kingdom

[g] Department of Mechanical Engineering, Indian Institute of Technology Kharagpur, Kharagpur 721302, India

[†] Authors have equally contributed to the work

[*] Current affiliation: Institute of Biomedical Engineering, University of Oxford, Old Road Campus Research Building, Oxford OX3 7DQ, UK. Email: dario.carugo@eng.ox.ac.uk

Abstract

Anticancer treatment using embolic drug-eluting beads (DEBs) has shown multifarious advantages compared to systemic chemotherapy. However, there is a growing need for a better understanding of the physical parameters governing drug-elution from embolic devices under physiologically relevant fluidic conditions. In the present study, we investigated the spatiotemporal dynamics of doxorubicin hydrochloride elution from drug-loaded hydrogel embolic beads within a microfluidic device~~,~~ consisting of a network of interconnected microchannels~~,~~ which replicates the architectural properties of microvascular systems. Drug-elution has been investigated experimentally at a single-bead level, using in-house developed microscopy- and spectrofluorimetry-based methods. Results demonstrated that the kinetics of drug-elution and the amount of eluted drug strongly depended on the location of the embolic event within the embolised channel (e.g. fractional amount of eluted drug after 3 hours was equal to ~0.2 and ~0.6 for completely-confined and partially-confined bead, respectively). Drug-elution from partially-confined bead showed a counterintuitive dependence on the local Reynolds number (and thus on the mean fluid velocity), as a result of dynamic changes in bead compressibility causing the displacement of the bead from the primary embolic site. Conversely, the kinetics of drug-elution from fully-confined bead was less affected by the local Reynolds number and bead displayed faster elution from the surface area exposed to the systemic flow, which was associated with the formation of fluid eddies nearby the bead post embolisation.

Keywords: Chemoembolisation, Embolisation, Drug-elution, Hydrogel bead, Doxorubicin hydrochloride, Microchannel network, Microfluidics, Hydrodynamics.

1. Introduction

Traditional cancer chemotherapy suffers from major limitations, mainly originating from its systemic nature [1, 2]. In order to overcome these, locoregional therapies have been achieved by different physical and bio-chemical means, encompassing ablation-, radiation- and embolisation-based techniques, potentially in combination with the administration of bio-active compounds. Notably, targeted drug delivery has been associated with increased drug concentration ~~to~~ within

the tumour and reduced systemic exposure [3, 4]. Transarterial chemoembolisation (TACE) has been used for over 30 years and is performed by local arterial infusion of the chemotherapeutic agent and subsequent injection of embolic particles [5]. Thus, it synergistically combines tumour starvation caused by embolisation [6, 7], with the cytotoxic effect of drugs whilst minimising the systemic toxicity [8, 9]. TACE has been demonstrated to be particularly effective for treating hypervascularised tumours and especially hepatic malignant lesions, which derive their main blood supply from arterial vessels [5]. Whilst the advantages of TACE with respect to systemic chemotherapy have been widely demonstrated [10-12], there still persists a lack of method standardisation among clinicians in terms of properties of the embolic device and administration techniques to be employed for achieving a desired therapeutic effect [5, 13]. In order to address these issues, drug-eluting beads (DEBs) in the form of calibrated deformable microspheres have been introduced as embolic devices [14]. DEBs are generally biocompatible, non-degradable polymeric spheres loaded with specific molecules (i.e., anticancer drugs) which are released for prolonged time after injection and vessel occlusion [8, 11, 15, 16]. This allows spatially controlled and simultaneous delivery of the anticancer drug and the embolic device in a single step, by means of microcatheters [7, 17], providing improved controllability and reduced rate of trans-hepatic clearance compared to conventional TACE [5]. In addition, patients treated with DEBs have shown increased mean survival compared to systemic chemotherapy [16, 18-20] and reduced peak plasma concentration compared to conventional TACE [5]. Therefore, DEB-based chemoembolisation is regarded as an appealing therapeutic strategy for treating tumours which are not eligible for other curative treatments such as laser ablation or resection [21-25].

DC Bead® is a microspherical drug delivery embolisation device [15] which consists of a polyvinyl alcohol (PVA) polymer hydrogel which has been modified by addition of a sulfonic acid-containing component. This device is capable of actively sequestering oppositely charged molecules (i.e., doxorubicin hydrochloride) by ion-exchange mechanism [26], and subsequently

releasing them when exposed to Na^+-rich fluidic environments (i.e., blood plasma) [27, 28]. DC Bead® is formulated by inverse suspension polymerisation [29], and is supplied in different diameter ranges from 70 μm to 700 μm [27], the selection of which will depend on the diameter of the vessel to be occluded [30, 31].

It has been previously demonstrated that DEBs' performance strongly depends on bead size distribution [5, 17], chemical composition [32] and the amount of loaded drug [17]. These parameters will, in turn, affect bead mechanical properties [17] and deliverability *via* microcatheters. Furthermore, we have previously demonstrated that the fluid dynamics within the target vascular system can influence the flow behaviour of suspended embolic beads [33] and, ultimately, determine the spatial location of vascular occlusion sites [34]. The spatial location of embolic events has been observed to further depend on bead size and concentration in the embolic suspension, which was previously postulated by others but only qualitatively [35]. Additionally, it has been shown that embolisation with hydrogel beads happened in the form of proximal multi-bead occlusion or distal single-bead occlusion, indicating distinct therapeutic implications [34, 35]. Notably, single-bead occlusion is desired as it is associated with more efficient devascularisation [35] and generally generates confined tissue ischaemia. Proximal vascular occlusion may instead result in non-targeted tissue ischaemia and off-target delivery of chemotherapeutic agents [36].

Currently, the evaluation of drug-elution kinetics from DEBs is performed by using a range of different apparatuses. Classical set-up for dissolution tests consists of a reactor where beads are positioned and the fluid is perturbed by a rotating paddle (i.e., USP II apparatus) [5]. While it is useful for comparative analyses between different chemoembolic devices, this set-up does not mimic the fluid dynamic environment surrounding the embolic beads *in vivo* and cannot be used to characterise long-term drug release [37, 38].

An experimental apparatus was developed by Amyot *et al.* (2002) which consisted of a T-shape device with a driven cavity where beads were positioned. This system, also called "T-apparatus" [37], reproduced more closely the *in-vivo* hydrodynamic environment compared to systems previously available. Notably, drug-elution experiments performed using the T-apparatus displayed good *in-vitro in-vivo* correlation (IVIVC) [7, 28]. However, despite remarkable progress in the design of biomimetic *in-vitro* systems for drug-elution studies, there is no widely accepted standard system developed for studying drug-elution from embolic beads [28]. This is primarily due to the fact that current experimental apparatuses are not capable of reproducing the intricate architecture of tumour vascular networks [39], which prevents effective simulation of the complex phenomenology involved in actual embolisation and elution processes. In addition, embolic beads are generally lodged within a dissolution chamber [28], in which they do not experience any deformation or confinement as would be experienced *in vivo*.

It is, therefore, important to develop novel experimental strategies allowing for the investigation of drug-elution kinetics from embolic beads under physiologically relevant fluidic conditions, in which beads are restrained within a confined fluidic domain (i.e., biomimetic embolisation) [7, 34].

In the present study, the elution of doxorubicin from hydrogel embolic beads has been investigated within a microchannel network which reproduced typical features of tumour microvascular systems. The device exploited advantages provided by microfluidic technology, including fine control over the boundary conditions [40], manipulation and monitoring of micro-scale objects [41], and flexible interfacing with analytical and optical instruments [42]. In our previous study we demonstrated that this device allowed for a faithful reproduction of embolisation mechanisms and phenomenology [34], and we employed it to investigate the effect that the flow dynamic field exerts on the spatial distribution of embolic beads within

microchannel networks and, in turns on the location of embolic events. In the presents study, we instead focused on the elution mechanisms from drug-loaded beads.

The commercially-available drug eluting embolisation system DC Bead™ loaded with doxorubicin was selected for our investigations and our experimental hypothesis based upon the desire to understand the effects of embolisation location and flow dynamic field on drug elution characteristics. The elution of doxorubicin from a single embolic bead was quantified *on-chip* using *in-situ* fluorescence microscopy. This allowed for the non-invasive determination of relevant information regarding the spatial and temporal evolution of drug-elution from embolic beads, under a range of different fluidic conditions. The role played by the location of the occlusion site (i.e., partial or complete bead confinement in the occluded vessel) on the release process could be evaluated. *Off-chip* continuous-flow spectrofluorimetry measurements were also performed in order to validate microscopy-based observations and further predict the spatial distribution of eluted free-drug within microchannel networks, a relevant topic in chemoembolisation research.

2. Materials and Methods

2.1 Materials

DC Bead® (300-500 μm in diameter) was provided by Biocompatibles UK Ltd (Farnham, UK). Physiological buffered saline solution (PBS) and doxorubicin hydrochloride were purchased from Sigma-Aldrich Co. (Gillingham, UK). 1 μm diameter polystyrene microspheres conjugated with fluorescein isothiocyanate were purchased from Polysciences Inc. (Warrington, US). Deionised water was purchased from EMD Millipore (Billerica, US).

2.2 Design and fabrication of microfluidic networks

The procedures used for microfluidic device design and fabrication have been extensively described in our previous works [34, 43]. Briefly, the microchannel network was designed in AutoCAD (Autodesk Inc., US). Network architecture consisted of two generations of microchannels and was characterised by enhanced spatial asymmetry and severe reduction of channel inner diameter occurring in few generations, as observed in tumour arterial vascular systems, either in human or in animal models [44, 45]. Network architecture thus consisted of segments with various hydraulic resistance, generally classified as low-resistance segments and high-resistance segments [36], each carrying a distinct amount of fluid and beads over time [34]. Importantly, microchannel cross-sectional area fell into the range of small arteries and arterioles, which generally correspond to the vascular domain targeted by microcatheter-injected embolic beads [34]. Within the constructed architecture, channel inner diameters varied from 1000 μm (proximal) to 200 μm (distal).

Microchannels were fabricated by micromilling technology (Datron CAT3D-M6, Datron Dynamic Inc., US). Ball-nose mill bits were employed to transfer geometry architecture into two highly transparent polymethyl-methacrylate (PMMA) layers. The milled polymeric layers were then aligned and bonded together in order to obtain microchannels with circular cross-section (inset, Fig. 1). Finally, connection ports with 1/4-28 flat-bottom thread were created on the side of the device, in order to join the end of each channel with 1/16'' OD tubing (IDEX Health & Science Llc, US) for working fluid delivery and release.

2.3 Samples preparation

DC Bead® (300-500 μm) (Biocompatibles UK Ltd, Farnham, UK) was loaded with doxorubicin hydrochloride (Zhejiang, China, dose density: 37.5 mg/mL of hydrated beads), according to the manufacturer's instructions for use. The product was supplied lyophilised for these studies and

hydrated prior to use with deionised water (Millipore, US). Samples were at ambient temperature during experiments (~21ºC).

2.4 Experimental set-up and bead injection protocols

Fig. 1 shows the schematic of the experimental set-up used for drug-elution experiments. The working fluid was pumped from a 50 mL capacity reservoir (systemic reservoir, SR) and conveyed into the microfluidic device *via* 1.3 mm ID silicone tubing (arterial line, AL) using a peristaltic pump (Watson-Marlow Pumps Group, UK). A pressurised glass cylinder (Fisher Scientific Inc., UK) partially filled with physiological buffered saline solution (PBS, pH = 7.2, Sigma-Aldrich Co., UK) was positioned between the pump and the microfluidic device; assuring the dampening of the flow pulsatility (i.e., a steady flow was achieved).

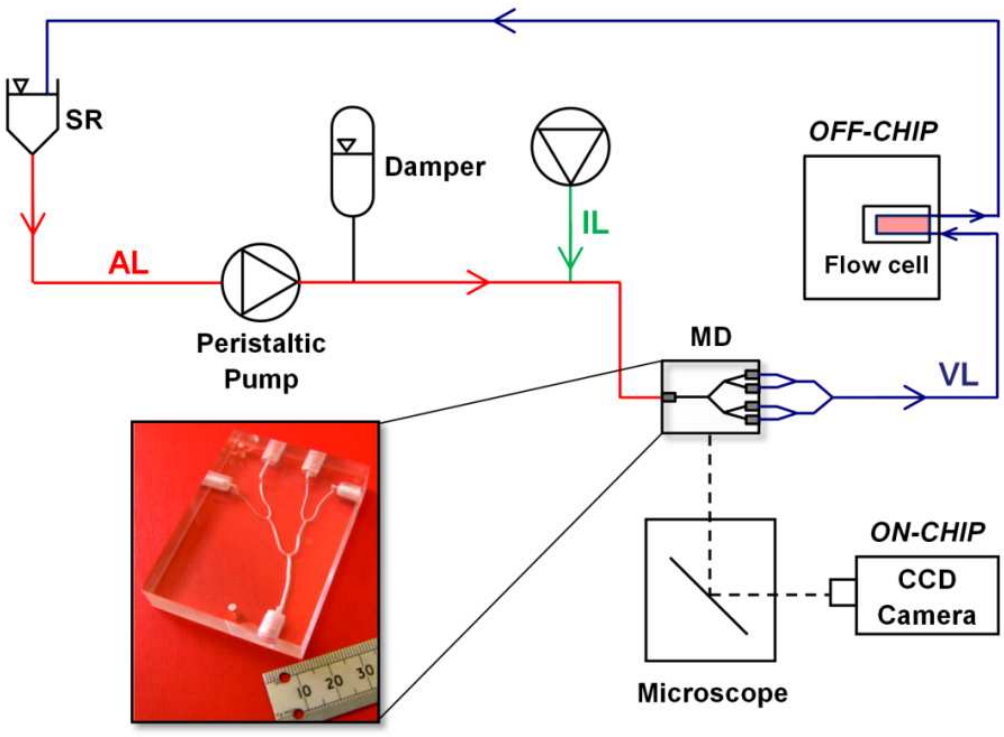

Fig. 1. Schematic of the experimental set-up designed for doxorubicin elution studies from single embolic hydrogel bead. The working fluid is pumped from the systemic reservoir (SR) by a peristaltic pump. The pump is followed by a damper for achieving steady flow condition. The flow is conveyed into the microfluidic device (MD) and redirected into the SR via the venous line (VL). An *ad hoc* injection line (IL) has been designed for bead injection into the AL. Either ON-CHIP analysis or OFF-CHIP analysis

can be performed using the developed set-up. (Inset) Photograph of the polymethyl-methacrylate (PMMA)-based microfluidic device.

PBS was selected as the working fluid, to correlate with conventional dissolution kinetics experiments [7, 27]. In addition, PBS mimicked the osmotic and electrolytic environment to which beads are exposed within the vasculature. The working fluid had a density (ρ_f) of ~1020 kg/m^3 and dynamic viscosity (μ_f) of ~0.001 Pa·s.

The inlet volumetric flow rate (Q_{in}) was set between 3.3 mL/min and 13.2 mL/min, corresponding to a selected range of physiological Reynolds numbers (Re_{in}) between 71.28 and 287.28 within the feeding channel (channel A, Fig. 2a) [46]. These corresponded to mean fluid velocities (V_{in}) in the range 7.13-28.73 cm/sec, which are comparable with those observed in tumours [47, 48]. We varied V_{in} so as to account for the large variability in the fluid dynamic conditions which is typical of tumour vascular systems [49, 50]. Re_{in} represents the ratio of inertial forces to viscous forces, and was calculated as follows:

$$\mathrm{Re}_{in} = \frac{\rho_f V_{in} D_{in}}{\mu_f} \quad (1)$$

where V_{in} is the average fluid velocity in the feeding channel (channel A) and was determined as $V_{in} = Q_{in}/[\pi \cdot (D_{in}/2)^2]$, where D_{in} is feeding channel inner diameter (D_{in} = 1000 μm).

After passing through the microfluidic device, the working fluid was conveyed into the systemic reservoir *via* silicone tubing representing the venous line (VL). The priming volume for the above described set-up corresponded to 50 mL, thus assuring doxorubicin concentration to be below the solubility limit in water, which is equal to 10 mg/mL [51], whilst ensuring its

detectability by fluorescence spectroscopy, which has a limit of detection (LOD) of 2.0 μg/L [52].

A single microsphere was isolated from the suspension of beads using a micropipette and injected into the arterial line *via* an *ad hoc* injection line (IL, Fig. 1) using a gastight 5 mL capacity glass syringe (Hamilton Company, Switzerland).

2.5 In-vitro embolisation protocols

Following injection, the single bead was transported by the fluid flow towards a point where channel diameter was small enough to impede any further distal transition within the network; this procedure resulted in single-bead embolisation within the microchannel network. Embolisation was achieved at different locations within the microvascular network, which were classified as *partially-confined* (near the bifurcation point in channel C2) and *completely-confined* embolisation modalities (fully confined within channel C3) (Fig. 2a). This was achieved by selectively clamping the tubing constituting the VL, thus controlling the hydraulic resistance in such a way to direct the bead towards the desired site within the network.

Partially-confined embolisation was characterised by incomplete penetration of the bead within the embolised channel (Fig. 2b), resulting in partial exposure of the bead surface to the systemic fluid flow. Conversely, completely-confined embolisation was characterised by complete penetration of the bead within the embolised channel (Fig. 2c). These two distinct embolisation modes were assessed and discriminated by optical microscopy.

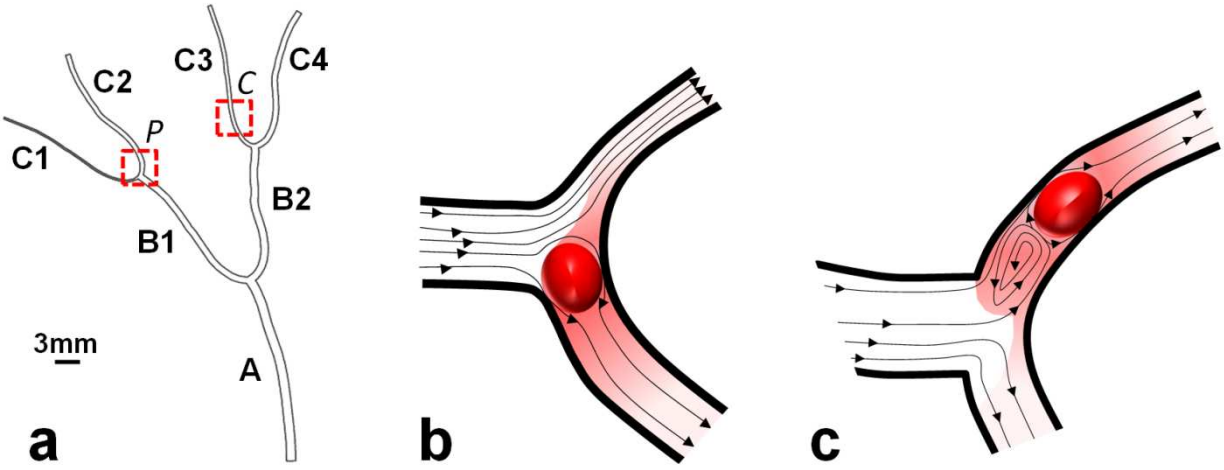

Fig. 2. (a) Computer Assisted Design (CAD)-based schematic of the microchannel network design (scale bar: 3 mm). Channel inner diameters: dA = 1000 μm, dB1 = 700 μm, dB2 = 800 μm, dC1 = 200 μm, dC2 = 500 μm, dC3 = 400 μm, dC4 = 600 μm. Spatial locations of partially-confined (P) and completely-confined (C) embolic events are reported (red squares). Partially-confined embolisation resulted in partial penetration of the bead in the embolised channel, associated with partial bead exposure to the systemic fluid flow (b). Conversely, completely-confined embolisation resulted in complete penetration of the bead in the embolised channel (c).

2.6 On-chip analysis

Prior to the embolisation procedure, the microfluidic device was fixed on the stage of an inverted fluorescence microscope (IX71, Olympus Corporation, Japan), coupled with a 1392×1040 pixels×pixels high-speed CCD camera (QICAM Fast 1394, QImaging, Canada; equipped with Sony® ICX205 progressive-scan interline CCD) and a personal computer (PC) with image acquisition software Image-Pro Insight (Media Cybernetics, Inc., US) (Fig. 1). This allowed the monitoring of the embolisation procedure and efficient data transfer for subsequent image processing.

2.6.1 Quantification of drug-elution

After single-bead embolisation was achieved (Supplemental Fig. S1.1), the bead was exposed to fluorescent light (excitation wavelength, λ_{ex} = 480 nm) and emitted light with a wavelength, λ_{em},

of 580 nm. A 200 W metal arc lamp (Lumen 200, Prior Scientific, US) set at 100% light output was employed in the present study. Detector gain and gamma function were set to the default values (i.e. equal to 1). Optical parameters were kept constant throughout experiments, including both drug elution and fluorescence calibration tests, as for previous studies [53, 54].

The bead was exposed to the fluorescence light solely during the image acquisition time (i.e., 100 ms) in order to minimise photobleaching.

By using an appropriate optical filter (see full details about excitation and emission filters' specifications in Supplementary section S3.1), only the spatial domains containing doxorubicin hydrochloride appeared on the acquired images, with a light intensity level proportional to the amount of drug present (Supplemental Fig. S1.1). Microscope focus was set on the microchannel mid-plane and multiple image frames (10× magnification, Olympus Plan Fluorite Objective, 0.3 Numerical Aperture (NA) = 0.3, Working Distance = 10 mm) were acquired with inter-frame time interval of 1-2 min, for a total acquisition time ranging from 3 hrs (short-term elution) to 20-24 hrs (long-term elution). The depth of focus in our experiments was estimated to be 266.67 μm (see Supplementary section S3.2), corresponding to a significant fraction of the bead. Video 1 illustrates a representative microscope image sequence of the fluorescence signal from a single, completely-confined bead.

The acquired images were processed in an automated fashion by using an in-house software developed in MATLAB R2011a environment (The Mathworks Inc., US) (Fig. 3). In order to quantify the fractional amount of drug eluted from a single embolic bead, the time reduction of fluorescence intensity on the bead surface (*FI*) was determined. Notably, areas of no interest for image processing purposes were excluded from the analysis, thus reducing the computational cost. *FI* was observed to reduce with time, due to the elution of drug from the bead to the outer working fluid. The amount of eluted drug from the bead was calculated by converting *FI* values into mass values (in μg). For this purpose, solutions of doxorubicin hydrochloride in PBS, at

known concentrations, were injected within the microfluidic device and the corresponding *FI* values were quantified from acquired microscope images (see Supplementary section S2 for more details about fluorescence intensity calibration and quantification of drug elution).

The fractional amount of eluted drug (ϕ) was determined as follows:

$$\phi(t) = 1 - \frac{M(t) - M(t_{end})}{M(t_0) - M(t_{end})} \quad (2)$$

where $M(t)$ is the amount of drug at a given time instant t, $M(t_0)$ is the initial amount of drug (at $t = t_0$) and $M(t_{end})$ is the amount of drug at the end of the analysed elution process (at $t = t_{end}$). $M(t_0)$-$M(t_{end})$ thus corresponds to the amount of eluted drug from time t_0 to time t_{end}. It should be noted that the definition of fractional amount of eluted in this study may not correspond to the conventional one, but it was deemed suitable for comparison between different embolic modalities and analysis techniques.

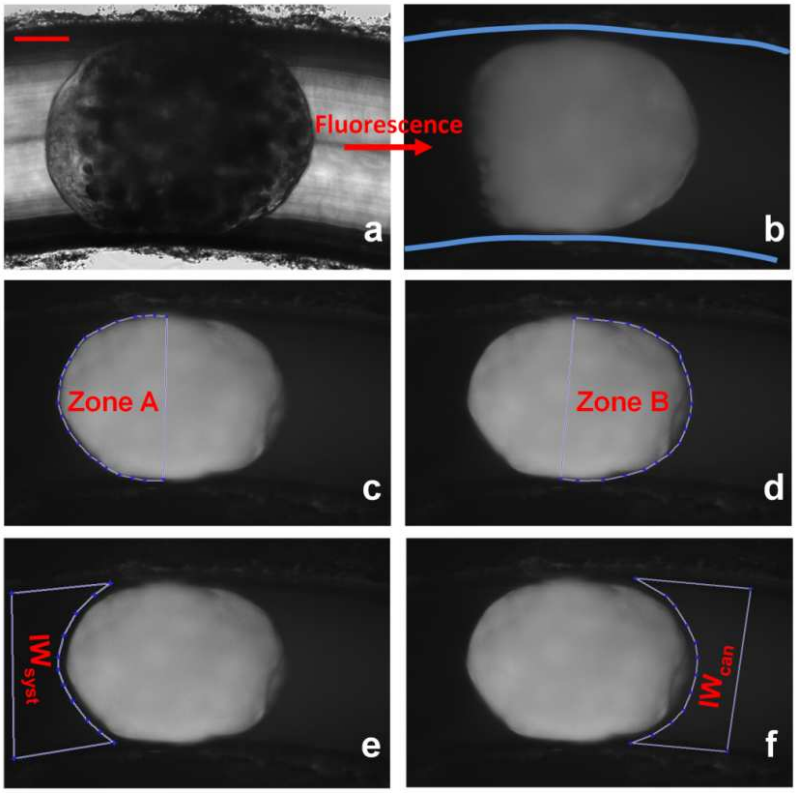

Fig. 3. On-chip analysis of drug-elution from single hydrogel bead. (a) Representative bright field microscope image of a single DC Bead® (completely-confined embolisation, channel C3), at t = 21.5 hrs from the embolic event (red line = 100 μm). (b) Corresponding fluorescent image, showing the spatial distribution of doxorubicin hydrochloride over the bead surface. The blue line in (b) indicates the channel inner wall. Drug-elution was determined from either the total bead surface or from a selected region of interest on the bead surface, identified as Zone A (c) and Zone B (d). Two *IWs* were also defined nearby the bead in order to quantify the spatial distribution of eluted drug, which were identified as IW_{syst} (e, towards the systemic flow) and IW_{can} (f, towards the target cancer tissue). *IW* = Interrogation Window.

With the developed computational analysis system, a doxorubicin elution profile could be determined from either the total bead surface or from a specific domain of interest on the bead surface (Fig. 3). The contribution of photobleaching (i.e., fluorescence intensity reduction) due to multiple excitation cycles was taken into consideration during image analysis.

Additionally, contours of fluorescence intensity on the bead surface were determined computationally, providing unique spatial information regarding the elution process. These correspond to a coloured representation of the experimentally-acquired fluorescence intensity signal over the entire image frame. Notably, bead surface area was divided into two distinct domains which were exposed to different hydrodynamic conditions at the embolic site. These hydrodynamic regions were characterised by (i) direct exposure of the bead surface to the systemic fluid flow (in case of partially-confined embolisation) or to fluid flow perturbations resulting from the embolic event (in case of completely-confined embolisation) (zone A, Fig. 3c), and (ii) a significant reduction of fluid flow due to the embolic event (zone B, Fig. 3d). Flow patterns were visualised by using 1 μm diameter polystyrene fluorescent tracers (Polysciences Inc., US, conjugated with fluorescein isothiocyanate) suspended in the working fluid at a concentration of 0.1% by volume.

In addition, the maximal amount of eluted drug at a given time instant ($t = t_{end}$) normalised with respect to the initial mass (at $t = t_0$) was calculated as follows:

$$\Delta M_{\max} = \frac{|M(t_{end}) - M(t_0)|}{M(t_0)} \quad (3)$$

2.6.2 Quantification of bead displacement

The mechanical properties of PVA hydrogel beads (i.e., Young's modulus) have been observed to significantly change after loading with anticancer drugs, such as doxorubicin hydrochloride [17]. It is thus expected that DEBs undergo a dynamic variation of their mechanical properties *in vivo* [7], likely due to the uptake of water and structural changes in the architecture of the polymeric network [17] associated with the drug-elution process. In particular, increased bead deformability can potentially lead to the dislocation of the bead from the initial embolic site (primary embolic event) and its displacement towards a more distal region within the vascular system (secondary embolic site), thus dynamically influencing the kinetics of the drug-elution process.

In order to quantify elution-induced bead displacement, the bead position within the microchannel network was dynamically determined through image analysis. Following the ratio between bead surface area in zone A (A_A, in pixel^2) and bead surface area in zone B (A_B, in pixel^2) an area partitioning coefficient (α) was defined:

$$\alpha(t) = \frac{A_A(t)}{A_B(t)} \quad (4)$$

α was calculated computationally in an automated fashion.

A distal movement of the bead would therefore correspond to a reduction in A_A, and thus a reduction in partitioning coefficient (α).

2.6.3 Spatial distribution of eluted drug

In order to further investigate the spatial distribution of eluted drug from the bead, two equally-sized interrogation windows (*IWs*) were defined adjacent to the bead surface, using the in-house developed computational analysis system. The distance between bead centroid and *IWs* centroid was high enough to ensure that the *IWs* did not overlap with the bead surface.

One *IW* was positioned just prior to the embolic bead (IW_{syst}, Fig. 3e), whilst the second *IW* was positioned just after the embolic bead (IW_{can}, Fig. 3f). The mass of drug within each *IW* was determined and the ratio $\beta(t) = M_{can}(t)/M_{syst}(t)$ was calculated, where M_{syst} is the mass of drug in IW_{syst}, which provided a prediction of the amount of eluted drug directed towards the systemic circulation. M_{can} is the mass of drug in IW_{can} and provided a prediction of the amount of drug eluted towards the target cancer tissue. $\beta(t)$ thus provided a quantitative measurement of the on-time preferential direction of the eluted drug, at the different Re_{in} investigated.

2.7 Off-chip analysis

The venous line was connected to a quartz flow cell (path length: 1 mm, 73.4-F, Starna Scientific Ltd., UK) for continuous spectrofluorimetric analysis. In this method, drug eluted from the embolic bead was quantified in the quartz cell. The working fluid was conveyed into the flow cell for analysis and subsequently conveyed into the systemic reservoir (Fig. 1), thus assuring flow to be recirculated.

2.7.1 Quantification of drug-elution

A spectrofluorimeter (Cary Eclipse, Varian, Agilent Technologies Inc., US) was employed for quantification of doxorubicin elution from single bead occluding a microchannel. The fluid containing doxorubicin was exposed to fluorescent light at λ_{ex} = 480 nm. The emitted light in the wavelength range 520 nm – 650 nm was detected and its intensity acquired every 2 min. The total acquisition time was set to 24 hrs.

A computational-based data processing platform was designed in MATLAB environment for automated processing of the experimental data. The developed software read the emitted light intensity profiles and extracted the peak intensity at a fixed wavelength, λ_{em} = 580 nm. The contribution of photobleaching, due to multiple excitation cycles over time, was taken into consideration during data analysis.

The fractional amount of eluted drug was determined by calibration with solutions of doxorubicin hydrochloride in PBS, at known concentrations (as described in paragraph 2.5.1).

ϕ was calculated as follows:

$$\phi(t) = \frac{M(t) - M(t_0)}{M(t_{end}) - M(t_0)} \quad ; \quad \text{with} \quad M(t_0) = 0 \tag{5}$$

where, analogously to Equation 2, $M(t_{end})$-$M(t_0)$ represents the total amount of eluted drug.

3. Results and Discussion

3.1 Functional and phenomenological observations

The developed microfluidic device allowed for the replication and *in situ* monitoring of peculiar phenomenological features of bead-induced vascular embolisation. Firstly, both embolisation generated by single bead and embolisation generated by multiple beads were investigated. As demonstrated in our previous study using unloaded hydrogel beads [34], multi-bead occlusion generally occurred in larger vessels [35] in the form of cluster-like structures with beads aligned along the channel axis or beads positioned in a zigzag-like pattern [34]; this is congruent with previous confocal microscopy-based analyses and angiographic acquisitions performed using animal models [55, 56].

In contrast, single-bead embolisation was observed in more peripheral channels within the microchannel network [56] with the bead conforming to the shape of the channel lumen,

resulting in tight contact between the bead surface and channel inner walls, which was coherent with previous microscopy-based experimental observations [5, 35] or post-embolisation histological analyses [56, 57] using animal models. Representative bright field microscope images of multi-bead and single-bead embolic events detected within the microchannel network are illustrated in Supplemental Fig. S1.1a and S1.1d, respectively.

Notably, due to device compactness and transparency, it was possible to couple microscope-based visualisation technology, with real-time quantification of drug content by exposure to fluorescent light, as illustrated in Supplemental Fig. S1.1b-c and S1.1e-f for representative multi-bead and single-bead embolisation, respectively. However, in the present study we focused on single-bead embolisation, which likely represents the more frequent form of peripheral microvessel occlusion using spherical embolic agents, as demonstrated by previous studies *in vivo* [11, 58-60]. Further to single- or multi-bead vascular occlusion, it was observed that single-bead embolisation happened in the form of either partially-confined or completely-confined occlusion, which was classified by the location of the embolic agent with respect to the occluded vessel (Fig. 2). Here, we defined partially-confined embolisation as an occlusive event localised in close proximity to the vessel inlet section, with the embolic agent partially occupying the bifurcating region. This modality of embolic event may occur in the case of severe reduction of vessel diameter from the parent vessel to the daughter vessels at a branching site, which is commonly observed in tumour vascular systems [61], or in any other situation in which bead diameter is significantly greater than vessel diameter (i.e., side-branch occlusion) (Fig. 2a). Notably, partially-confined embolisation was likely responsible for bead temporal crowding at bifurcations, which was observed *in vivo* using animal models, with either polyacrylonitrile hydrogel beads or dextran microspheres [56, 62].

We instead defined completely-confined embolisation as an occlusive event characterised by complete penetration of the bead within the vessel, away from the branching site.

Fig. 4 shows the average fractional amount of eluted drug from single bead (ϕ), at a fixed Re_{in} = 71.28, determined by off-chip analysis. Results from both partially-confined and completely-confined embolisation are reported, for preliminary comparative analysis between the two embolic modes detected within the network. Drug-elution was monitored quantitatively up to 21.5 hrs from the embolic event.

Firstly, results showed that the position of the embolic event within vascular networks significantly influenced the kinetics of the drug-elution from single hydrogel bead. Fig. 4 shows that ~~proximal~~ partially-confined embolisation generally caused burst-like elution of doxorubicin from single embolic bead, with the majority of the drug being eluted within the first few hours from the embolic event (i.e., ϕ = 0.55 after 3 hrs from the embolic event) and ϕ reaching a plateau level after ~ 10 hrs. We defined this elution kinetics as *short-term* elution. In contrast, ~~distal~~ completely-confined embolisation was observed to cause slower and sustained elution of doxorubicin during time, characterised by minimal burst-like elution within the first few minutes from the embolic event followed by constant elution rate. We defined this elution kinetics as *long-term* elution.

Notably, both elution profiles differed from those obtained using classical dissolution apparatuses (i.e., USP Type II), which were rather characterised by a faster elution kinetics in which the amount of eluted drug reached a plateau level after only 1 to 3 hrs from the embolic event, depending on bead size [27, 28]. Interestingly, drug-elution from completely-confined embolic bead displayed a qualitatively similar profile compared with that obtained using the T-apparatus set-up [28, 63], and conformed to experimental observations using animal models showing continuous drug-elution for prolonged time [10].

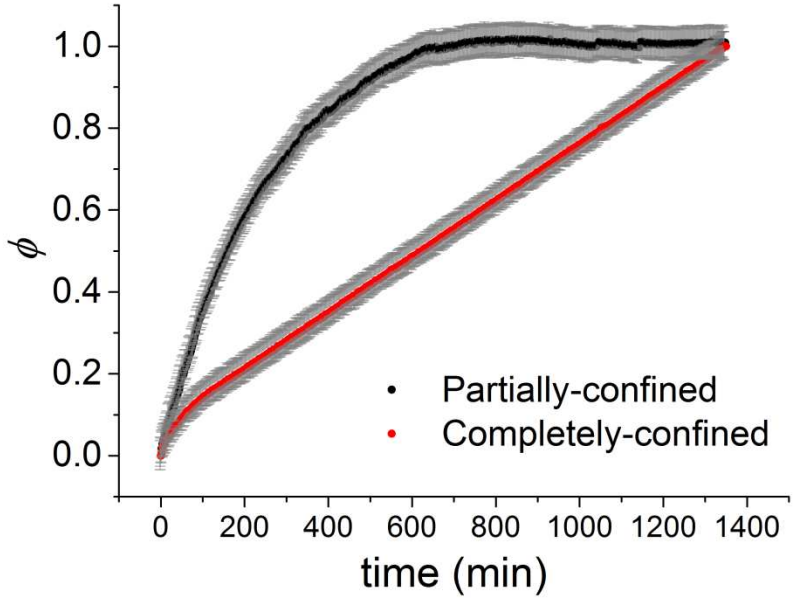

Fig. 4. Average temporal evolution of fractional amount of eluted drug (ϕ), for partially-confined embolisation (black circles) and completely-confined embolisation (red rhombi), determined by off-chip analysis. Re_{in} = 71.28 (corresponding to V_{in} = 7.13 cm/sec). t_{end} = 21.5 hrs. n = 3.

The two distinct elution profiles determined here revealed that different drug-elution kinetics may originate from differences in the location and the effectiveness of the embolic event. However, these differences cannot be captured by currently-available experimental apparatuses for studying drug-elution kinetics from embolic beads (i.e., USP Type II and T-apparatus); hence a more comprehensive understanding of the governing mechanisms under physiologically relevant fluidic conditions is required.

3.2 Comparison between on-chip analysis and off-chip analysis

Fig. 5 illustrates the comparison between drug-elution profiles (i.e., time evolution of fractional amount of eluted drug, $\phi(t)$) from single bead determined *via* on-chip analysis (ϕ_{OnC}) and off-chip analysis (ϕ_{OffC}). Average trends for partially-confined embolisation and ~~distal~~ completely-confined embolisation, at a fixed Re_{in} = 71.28, are reported. Fig. 5a shows the average ϕ_{OnC} and ϕ_{OffC} values for single partially-confined embolic bead (short-term elution). Good agreement between on-chip and off-chip experimental data can be observed in general, though on-chip data

appeared to be more scattered with respect to off-chip spectrofluorimetric acquisitions. For this purpose, ϕ_{OnC} and ϕ_{OffC} experimental data points have been interpolated with a Power Law function (adjusted-R^2 > 0.95 in all cases examined), and the corresponding interpolating functions have been plotted for comparison, as shown in Fig. 5b. Error bars (±10%·ϕ_{OffC}) have been determined and reported together with ϕ_{OffC} interpolating function to provide a measure of the agreement between off-chip and on-chip analysis methods. Results showed that for partially-confined embolisation, the interpolating ϕ_{OnC} function mostly fell within the range given by ±10%·ϕ_{OffC}. Higher discrepancies have been detected only in the first few minutes from the embolic event during which off-chip elution appeared to be slower than on-chip elution. This observation could be interpreted as the consequence of the intrinsic "inertia" of the off-chip analysis system in detecting the effective amount of eluted drug. Notably, a certain amount of doxorubicin was observed to be eluted towards the embolised channel (Supplemental Fig. S1.1d-e), where a drastic reduction of fluid flow occurred after embolisation. Therefore, it was likely that part of the drug released in the embolised channel did not reach the flow cell in the first few minutes post embolisation, hence it did not contribute to the amount of eluted drug detected through continuous spectrofluorimetric analysis. As a result, it was likely that the off-chip system was not capable of promptly detecting the initial elution of drug in the occluded channel. More experiments are underway in our laboratories to verify this hypothesis.

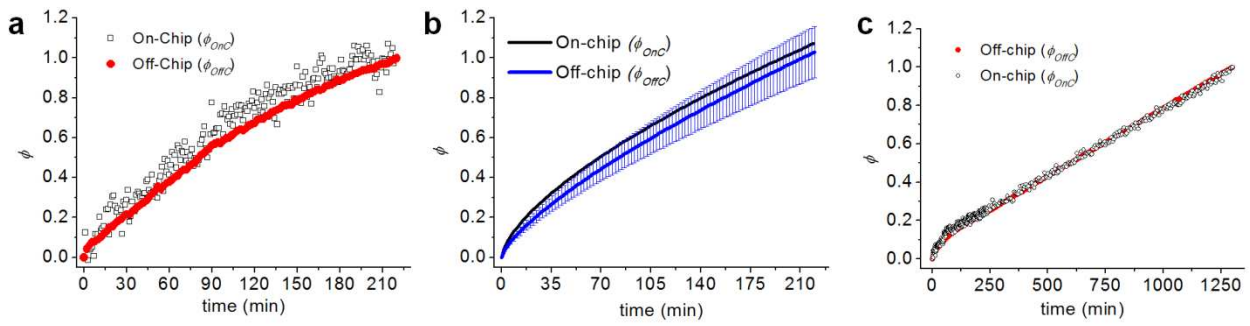

Fig. 5. Comparison between on-chip analysis and off-chip analysis. Average fractional amount of eluted drug determined by on-chip (ϕ_{OnC}) and off-chip (ϕ_{OffC}) analysis is reported for partially-confined embolisation (a) up to 220 minutes from the embolic event (short-term elution), and for completely-

confined embolisation (c) up to 1300 minutes from the embolic event (long-term elution). Comparison between interpolating ϕ_{OnC} and ϕ_{OffC} functions is reported for partially-confined embolisation (b). Error bars correspond to $\pm 10\% \cdot \phi_{OffC}$. n = 4. $Re_{in} = 71.28$.

Similarly, Fig. 5c reveals a good agreement between ϕ_{OnC} and ϕ_{OffC} experimental data for completely-confined embolisation (long-term elution). As observed for partially-confined embolisation, ϕ_{OnC} data points mostly fell within the range given by $\pm 10\% \cdot \phi_{OffC}$, and higher discrepancies between ϕ_{OnC} and ϕ_{OffC} values have been detected only in the first few minutes from the embolic event. Given the large number of data points, error bars have not been reported to allow clear interpretation of the graphs.

By direct comparison with commercially-available spectrofluorimetric instrumentation, results confirmed the validity of the on-chip analysis technique employed for measuring the kinetics of drug-elution from embolic beads within microfluidic channel networks. More importantly, both on-chip analysis and off-chip analysis techniques provided relevant information in the field of drug-elution from embolic devices, given that (i) *on-chip* analysis allowed for *in situ* visualisation of bead dynamic behaviour during the drug-elution process and the spatial distribution of the eluted drug, and (ii) *off-chip* analysis allowed for the quantification of drug distribution within network-like microchannel architectures which mimicked the fluid dynamics in the embolised vascular region occurring *in vivo*. It is worth mentioning that both techniques were non-invasive, i.e. no working fluid sample withdrawal was required, and they were particularly suitable for long-term continuous-flow drug-elution investigations. The aforementioned advantages allowed to overcome limitations associated with classical dissolution test methods employed in chemoembolisation research [28].

3.3 Effect of Reynolds number on drug-elution

3.3.1 Partially-confined embolisation

Fig. 6a shows the average temporal evolution of the fractional amount of eluted drug from single bead (ϕ), at the different Reynolds numbers investigated, as determined by on-chip analysis. This provides information regarding the role played by the fluid dynamic environment on the kinetics of drug-elution from single embolic bead. Data refer to short-term partially-confined embolisation only (i.e., t_{end} = 3 hrs), given the aforementioned preliminary considerations on drug-elution kinetics from partially-confined embolic bead, which eluted most of the payload within few hours from the embolic event. The total number of data points is equal to 180, corresponding to an inter-frame acquisition time interval of 1 minute. Fig. 6b instead shows the maximal amount of eluted drug (ΔM_{max}) after 3 hrs from the embolic event, which provides information on the amount of eluted drug from single embolic bead. Results showed that ϕ increased with time, as a result of drug-elution from the bead (Fig. 6a). Notably, the kinetics of drug-elution from single partially-confined bead was observed to be significantly influenced by the local fluid dynamic environment (i.e., Reynolds number in the feeding channel). In particular, at the lower Re_{in} (corresponding to lower mean fluid velocity), bead showed a relatively sustained and slow drug-elution during time (Fig. 6a), likely due to the lower fluid velocity and associated reduced drug advection. Increasing Re_{in} from 71.28 (V_{in} = 7.13 cm/sec) to 142.56 (V_{in} = 14.26 cm/sec) resulted in increased drug-elution within the first 40 min from the occurrence of the embolic event, corresponding to a faster kinetics (i.e., faster burst-like elution). Similar considerations applied when Re_{in} increased further from 142.56 to 213.54 (V_{in} = 21.35 cm/sec), likely due to increased drug advection at the higher Re_{in}, as mentioned previously. However, when Re_{in} increased from 213.54 to 287.27 (V_{in} = 28.73 cm/sec), the average drug-elution profile displayed a counterintuitive kinetics, characterised by sustained drug-elution rather than faster burst-like elution (Fig. 6a), as expected from conventional advection-diffusion theory. The normalised maximal amount of eluted drug (ΔM_{max}, Fig. 6b) displayed a similar dependence on

Re_{in} suggesting a non-linear relationship between the amount of eluted drug and the mean fluid velocity in the feeding channel.

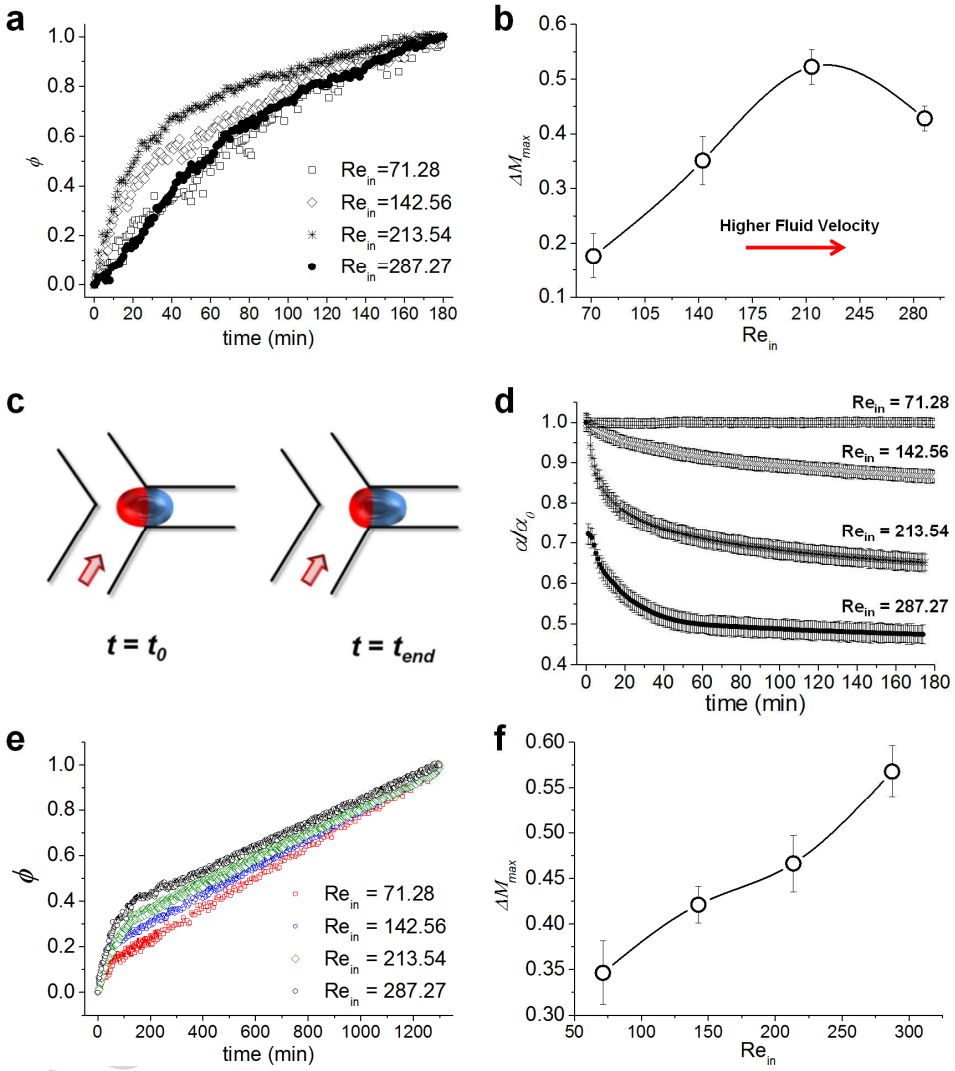

Fig. 6. (a-d) Effect of Reynolds number (or mean fluid velocity) on drug-elution from single partially-confined bead. (a) Average temporal evolution of the fractional amount of eluted drug (ϕ) for partially-confined embolisation, at different Reynolds numbers investigated. t_{end} = 3 hrs. n = 4, and standard deviation ranged from 1.25% to 8.89% of the mean. (b) Average maximal amount of eluted drug (ΔM_{max}) at the different Reynolds numbers investigated. t_{end} = 3 hrs. n = 4. (c) Schematic of bead penetration over time, within the embolised channel. The red area indicates Zone A and the blue area indicates Zone B. As a result of bead penetration, the area of Zone A decreases whilst the area of Zone B increases. The red arrow indicates the systemic flow direction. (d) Average temporal evolution of area partitioning coefficient (α), normalised with respect to $\alpha(t_0) = \alpha_0$, for the range of Reynolds numbers investigated. Symbols correspond to those of Fig. 5a. n = 4.

(e-f) Effect of Reynolds number (or mean fluid velocity) on drug-elution from single completely-confined bead. n = 4, and standard deviation ranged from 1.02% to 6.73% of the mean. (e) Average temporal

evolution of the fractional amount of eluted drug (ϕ) for ~~distal~~ completely-confined embolisation, at different Reynolds numbers investigated. t_{end} = 21.5 hrs. n = 4. (f) Average maximal amount of eluted drug (ΔM_{max}) at the different Reynolds numbers investigated. t_{end} = 21.5 hrs. n = 4.

Clearly, the aforementioned observations could not be captured by currently-available experimental apparatuses for studying drug-elution from embolic beads [28, 37]. More importantly, they cannot be explained with the conventional advection-diffusion theoretical paradigm, without taking into consideration the dynamic behaviour of the bead at the embolic site. In this respect, we provided a qualitative explanation based on quantitative experimental measurements.

Based on image analysis, the area partitioning coefficient (α) was calculated, which provided the on-time variation of bead surface area exposed to the fluid flowing from the feeding channel, with respect to the bead surface area penetrated within the embolised channel (Fig. 6c and Supplementary Figure S5.1). Fig. 6d shows the average temporal evolution of α, normalised with respect to $\alpha_0 = \alpha(t_0)$, at the different Reynolds numbers investigated. Results showed that at the lower $Re_{in} \leq 71.28$ (or $V_{in} \leq 7.13$ cm/sec) bead position remained substantially unvaried during time (i.e., $\alpha/\alpha_0 \sim 1$); whilst at $Re_{in} > 71.28$ (or $V_{in} > 7.13$ cm/sec), α/α_0 showed a decreasing trend, as a result of bead penetrating within the embolised channel, until a plateau value was reached, which corresponded to bead achieving a steady location within the embolised channel (see Supplementary Figure S5.1). The time reduction of α/α_0 was likely governed by the combined effect of increased hydrostatic pressure (driving force) at the higher fluid velocity, and the augmented bead deformability as a consequence of drug-elution, which synergistically contributed to the observed displacement of the bead. Thus, by increasing Re_{in} one would expect increased burst-like elution, particularly from the bead portion exposed to the fluid flowing from the feeding channel. Drug-elution in turn caused increased bead deformability (i.e., a dynamic

variation of bead mechanical properties occurred) and consequent bead penetration within the embolised channel under the effect of fluid forces (see Supplementary Figure S5.1). This indicated that the dynamics of the penetration process depended on both the amount of eluted drug (Fig. 6b) and the magnitude of hydrodynamic driving forces. This explains why α/α_0 displayed a more gradual reduction with time at the lower Re_{in} (i.e., $\alpha/\alpha_0 \sim 0.87$ after 3 hrs from the embolic event, at $Re_{in}=142.56$), which turned into a steeper reduction with increasing Re_{in} (i.e., $\alpha/\alpha_0 \sim 0.65$ and $\alpha/\alpha_0 \sim 0.48$ after 3 hrs from the embolic event, at $Re_{in}=213.54$ and $Re_{in}=287.27$, respectively), corresponding to increased drug-elution within the first few minutes after the embolic event occurred. Interestingly, the aforementioned counterintuitive variation in drug-elution kinetics at the higher Re_{in} (or fluid velocity) may be explained by the significant penetration of the bead into the embolised channel occurring within the first few minutes from the embolic event, likely resulting in reduced drug advection and consequent slowing-down of the elution process (i.e., bead was completely confined within the embolised channel at the higher Re_{in}).

In summary, the elution of doxorubicin hydrochloride from PVA hydrogel beads, in the case of partially-confined embolic event, displayed a complex and non-intuitive dependence of both drug-elution kinetics and the amount of eluted drug on the fluid dynamic environment. This likely originated from the dynamic behaviour of the bead at the embolic site and the interplay between fluid hydrodynamics and temporal variation of bead mechanical properties resulting from drug-elution and associated water uptake from the bead.

Results suggested that for partially-confined embolisation, in which bead was not completely penetrated within the embolised channel, drug-elution was strongly dependent on the mean fluid velocity in the feeding channel, which corresponded to the injection artery in the clinical scenario, thus suggesting that a more detailed prediction/control of blood flow within the target vasculature is required to better predict the elution performance of the injected embolic beads.

3.3.2 Completely-confined embolisation

Fig. 6e shows the average temporal evolution of the fractional amount of eluted drug from single completely-confined bead (ϕ), at the different Reynolds numbers (or mean fluid velocities) investigated, as determined by on-chip analysis. Data refer to long-term completely-confined embolisation (i.e., t_{end} = 21.5 hrs).

Similar to drug-elution from partially-confined bead, results showed that ϕ increased with time as a result of drug-elution from the bead (Fig. 6e). However, as anticipated, drug-elution from completely-confined bead was characterised by slow and sustained kinetics, with burst-like elution only limited to the first few minutes from the embolic event. By increasing Re_{in} we observed a longer burst-elution phase, which however reached a maximal duration of 100 min at the higher Re_{in} investigated. Burst-like elution was likely to be caused by release of drug at the bead surface [10].

Additionally, all elution profiles showed sustained and slow release after the first few minutes from embolisation. Interestingly, the elution rate did not change significantly with changing Re_{in}, thus suggesting that for completely-confined embolisation when bead was completely penetrated within the embolised channel, the kinetics of drug-elution from embolic bead was affected to a lesser extent by the mean fluid velocity in the feeding channel. These experimental observations may have multifarious clinical implications and suggest that effective penetration of the embolic bead is preferred, since it causes drug-elution kinetics to be less affected by the local haemodynamics in the target vasculature. Given that the exact location of vascular occlusion was observed to depend on a range of different physical parameters [5, 34] and it is thus difficult to predict it in the clinic, smaller diameter deformable hydrogel beads may be preferred since they generated effective distal occlusion [64]. In addition, Fig. 6f shows ΔM_{max} after 21.5 hrs from the embolic event. Results show that ΔM_{max} increased from 0.346 ± 0.035 at Re_{in} = 71.28 (V_{in} = 7.13

cm/sec) up to 0.568 ± 0.029 at Re_{in} = 287.27 (V_{in} = 28.73 cm/sec). As for drug-elution kinetics, the maximal amount of eluted drug was observed to vary less significantly with varying Re_{in}, and thus with varying the mean fluid velocity in the feeding channel, compared to partially-confined embolisation (i.e., ΔM_{max} spanned from a minimum of 0.17 to a maximum of 0.55, after only 3 hrs from the embolic event), further confirming that higher bead confinement led to the overall bead performance being less affected by the systemic flow dynamics.

3.4 Spatial distribution of drug over the bead

Contours of fluorescence intensity on the bead surface, as determined computationally by on-chip analysis, revealed the real-time spatial distribution of drug over the bead during the elution process. This allowed for high spatial- and temporal-resolution analyses of drug-elution mechanisms.

3.4.1 Partially-confined embolisation

Fig. 7 shows representative contours of fluorescence intensity on the bead surface, at the different Re_{in} investigated. Intensity values ranged from 0 to 256, where 0 corresponded to absence of drug and 256 corresponded to the maximum drug concentration. Contours at $t = t_0$, t = 70 min and t = 140 min are reported, for the range of Re_{in} investigated. The white dash-dot line in Fig. 7 provides a fixed reference frame for observation of bead dynamic motion.

Results showed that, in all cases examined, fluorescence intensity on the bead surface decreased with time, as a result of drug-elution from the bead towards the working fluid. Also, contours showed reduction of fluorescence intensity over the bead, with increasing Re_{in} up to 213.54 (corresponding to V_{in} = 21.35 cm/sec). However, as previously mentioned, such reduction of *FI* with increasing Re_{in} did not occur at $Re_{in} > 213.54$ (i.e., $V_{in} > 21.35$ cm/sec).

Additionally, beads were observed to elute drug in a relatively spatially-homogeneous way, with all bead surface visibly characterised by reduction in fluorescence intensity. In order to examine

the spatial nature of drug-elution from single bead, ΔM_{max} was quantified for either Zone A ($\Delta M_{max,A}$) located towards the systemic branch, and Zone B ($\Delta M_{max,B}$) located towards the embolised channel. Fig. 7o shows average values of $\Delta M_{max,A}$ and $\Delta M_{max,B}$ for the range of Re_{in} investigated. Results showed that either $\Delta M_{max,A}$ and $\Delta M_{max,B}$ values increased with increasing Re_{in} from 71.28 to 213.54. However, with increasing Re_{in} from 213.54 to 287.27, $\Delta M_{max,A}$ reduced from 0.646 ± 0.020 to 0.466 ± 0.039, likely due to enhanced bead penetration within the embolised channel (as illustrated in Fig. 7l-n), whilst $\Delta M_{max,B}$ slightly increased from 0.402 ± 0.037 (at Re_{in} = 213.54) to 0.433 ± 0.022 (at Re_{in} = 287.27) (Fig. 7o).

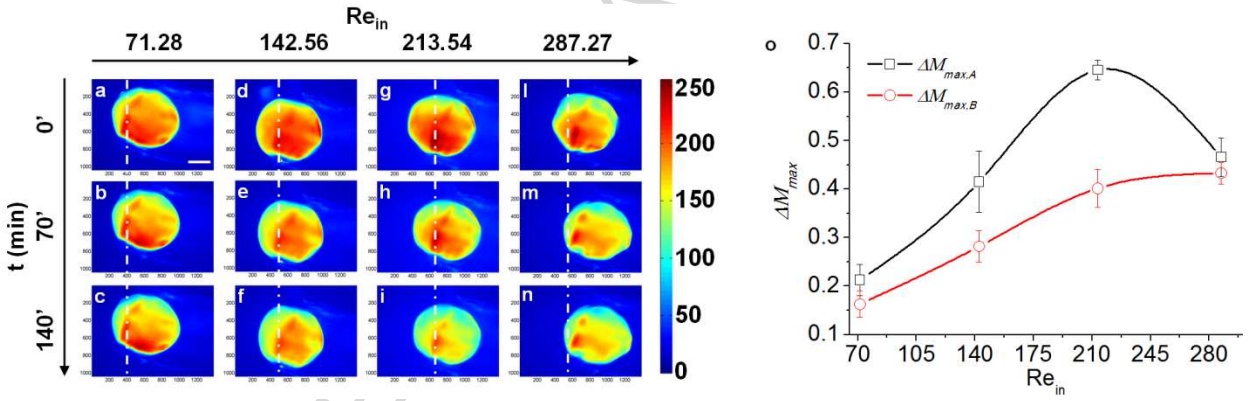

Fig. 7. (a-n) Contours of fluorescence intensity (intensity range: 0 – 256) for representative partially-confined single beads, at the different Reynolds numbers (or mean fluid velocities) investigated. Re_{in} = 71.28 (a-c), 142.56 (d-f), 213.54 (g-i) and 287.27 (l-n). Contours at $t = t_0$ (a, d, g, l), t = 70 min (b, e, h, m) and t = 140 min (c, f, i, n) are reported for the different Re_{in} investigated. The white dash-dote line provides a fixed reference system for observing bead penetration within the embolised channel, at the different Re_{in} investigated. White line in (a) = 150 μm. (o) Average maximal amount of eluted drug from Zone A ($\Delta M_{max,A}$) and Zone B ($\Delta M_{max,B}$) for partially-confined embolic bead, at the different Reynolds numbers investigated. t_{end} = 3 hrs. n = 4.

This suggested that by increasing Re_{in} up to a critical value (i.e., Re_{cr} ~ 213.54, corresponding to a critical mean fluid velocity V_{in} ~ 21.35 cm/sec) resulted in increased drug-elution, especially from the bead surface area exposed to the fluid flowing from the feeding channel (Fig. 7o).

However, when $Re_{in} > Re_{cr}$, the amount of eluted drug from this portion of the bead abruptly decreased likely due to higher bead confinement which impaired the elution process. From a clinical perspective, these observations may have implications on the spatial distribution of eluted drug within the vascular system, with increased elution from Zone A potentially contributing to increased less-targeted or systemic elution. Interestingly, experimental observations further revealed that when Re_{in} reached a critical value (corresponding to a critical mean fluid velocity) which caused complete bead penetration within the embolised channel, the extent of this phenomenon (i.e., faster drug-elution from Zone A) was markedly reduced, thus confirming the aforementioned counterintuitive dependence of drug-elution on Re_{in} as a result of bead dynamic behaviour (see Fig. 6a).

3.4.2 Completely-confined embolisation

Fig. 8 shows representative contours of fluorescence intensity on the bead surface, at different Re_{in} investigated, in the case of completely-confined embolisation. Contours at $t = t_0$, t = 6 hrs and t = 21.5 hrs are reported (long-term elution). Superimposed bright field and fluorescence images are also reported, showing the spatial distribution of doxorubicin over the bead at t = 21.5 hrs.

Similar to partially-confined embolisation, results showed that in all cases examined fluorescence intensity on the bead surface reduced with time, as a result of drug-elution from the bead. Contours also showed increased reduction of fluorescence intensity over the bead, with increasing Re_{in} and thus the mean fluid velocity. Interestingly, rather than a relatively spatially-homogeneous reduction of drug content over the bead, as observed for partially-confined embolisation, faster drug-elution was detected in Zone A, with some portions of the bead characterised by complete drug-elution after 21.5 hrs (Fig. 8c,f,i) (see Video 1 for a representative image sequence showing enhanced drug elution from Zone A). The physical mechanism behind this experimental observation was likely to be found in the onset of peculiar

hydrodynamics in close proximity to the bead surface as a consequence of the embolic event. In this respect, preliminary experimental observations using fluorescent tracers suggested the formation of laminar vortices nearby the bead (Fig. 9a and Video 2) in the case of effective completely-confined embolisation, with the position of the vortex centre, vortex size and fluid velocity likely depending on Re_{in} and the effectiveness of channel occlusion. From a fluid dynamic perspective this scenario can be ascribed to the category of 'flow past a cavity' problems, which has been thoroughly characterised either theoretically and experimentally [65, 66]. The first work to have elaborated a parallelism between the therapeutic embolisation of blood vessels and fluid flow within cavities was published by Amyot *et al.* in 2002 [37]. However, the implications of the fluid dynamic environment on the spatio-temporal dynamics of drug-elution from single bead have not been elucidated so far and, especially, at physiologically relevant fluidic conditions.

In order to investigate the spatial nature of drug-elution from single completely-confined bead, ΔM_{max} was quantified for either Zone A and Zone B. Fig. 8o suggests a non-linear dependence of the amount of eluted drug on Re_{in}, with $\Delta M_{max,A}$ displaying a significant increase at $Re_{in} \geq 142.56$ (corresponding to $V_{in} \geq 14.26$ cm/sec), likely due to aforementioned fluid dynamic scenario, in which vortex size and strength depended non-linearly on Re_{in}. Conversely, $\Delta M_{max,B}$ increased less significantly with increasing Re_{in}, thus suggesting that drug-elution within the embolised channel was less affected from the mean fluid velocity in the feeding channel, as a result of a more effective vascular occlusion for completely-confined embolisation which isolated the embolised compartment from the non-embolised or systemic compartment.

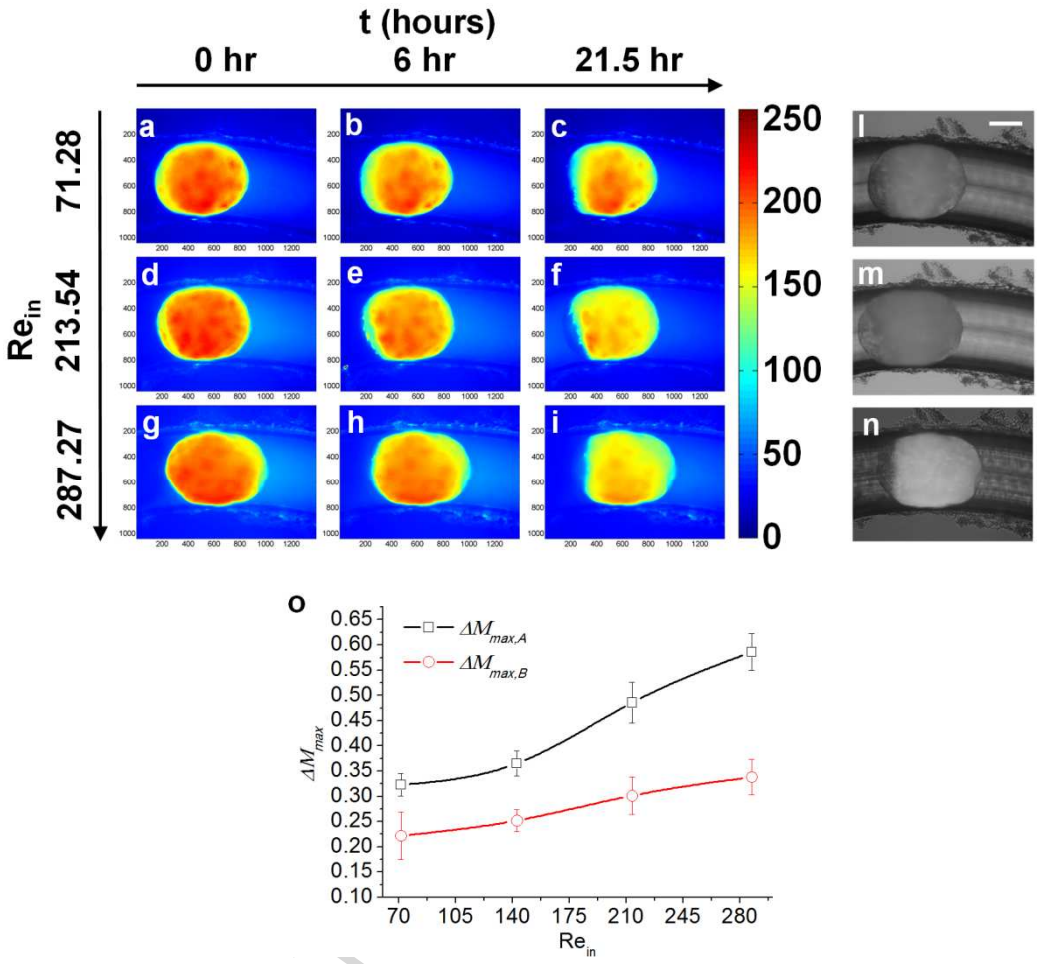

Fig. 8. (a-n) Contours of fluorescence intensity (intensity range: 0 – 256) for representative completely-confined single beads, at different Re_{in} = 71.28 (a-c), 213.54 (d-f) and 287.27 (g-i). Contours at $t = t_0$ (a, d, g), t = 6 hrs (b, e, h) and t = 21.5 hrs (c, f, i) are reported. Also, superimposed bright field and fluorescent microscope images are reported (l-n) at the different Re_{in}, showing the spatial distribution of the drug ~~within~~ over the bead at t = 21.5 hrs. White line in (a) and (l) = 150 μm. (o) Average maximal amount of eluted drug from Zone A ($\Delta M_{max,A}$) and Zone B ($\Delta M_{max,B}$) for ~~distal~~ completely-confined embolic bead, at the different Reynolds numbers investigated. t_{end} = 21.5 hrs (long-term elution). n = 4.

Results suggested that in the case of completely-confined embolisation, drug-elution from single embolic bead displays unique features, including faster drug-elution from the bead surface area oriented towards the feeding channel. Notably, complete penetration of the bead in the embolised channel caused the formation of laminar vortices in the newly formed cavity (Figure 9 and Video 2), which may potentially cause the observed spatially inhomogeneous elution of drug from the

bead (i.e., vorticity-enhanced diffusion). Further numerical and experimental investigations are currently being performed in our laboratories in order to better understand and characterise this phenomenon.

In addition, completely-confined beads did not displace from the primary embolic site, as for partially-confined embolic bead at the higher Re_{in} (corresponding to higher mean fluid velocities in the feeding channel), providing a stable and durable vessel occlusion.

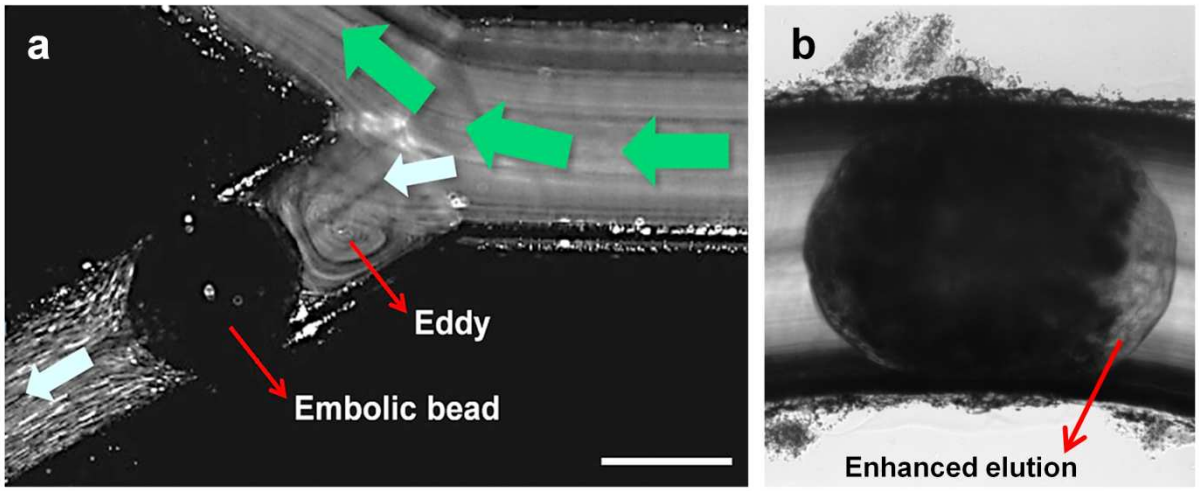

Fig. 9. (a) Representative microscope image of 1 μm diameter fluorescent tracer particles flowing within the microfluidic device, in close proximity to the embolic event. Green arrows indicate the systemic flow direction, whilst light blue arrows indicate the presence of residual fluid flow rate in the embolised channel. Eddy formation within the embolised channel, in close proximity to the embolic bead, is clearly detectable. Scale bar: 500 μm. (b) Bright field microscope image of single embolic bead showing enhanced drug-elution from the bead surface area exposed to the fluid eddy.

4. Conclusions

The optimisation of chemoembolisation devices and related administration techniques requires a more comprehensive understanding of the physical mechanisms governing the process of drug-elution from embolic devices. This can be beneficial for further minimising the occurrence of

undesired side-effects on the treated patients, achieving better control on the treatment clinical outcome, and designing novel therapeutic strategies.

Currently, the evaluation of drug-elution kinetics from embolic beads is performed by using *in-vitro* test methods which do not replicate the intricate architecture of vascular and microvascular systems and, importantly, do not allow for the mimicking of the phenomenology of the embolisation process, which is characterised by a range of potentially different dynamic behaviours.

In the present study we have described a novel microfluidic technique for investigating the elution of anticancer drugs from hydrogel embolic beads. With this technique, we assessed whether embolisation location and fluid dynamic field contributed to the spatial and temporal characteristics of the elution process, which was the driving hypothesis for the present study. Both on-chip and off-chip experimental methods have been implemented for this purpose, together with automated computational-based analysis systems for rapid quantification of drug-elution profiles and a range of other related parameters. Notably, the on-chip analysis method represents a novel way of quantifying non-invasively drug-elution from embolic devices in order to get high resolution temporal and spatial information regarding the elution process from a single embolic bead, *via* coupling with microscope systems.

With the developed technology we have investigated the mechanisms of elution of doxorubicin hydrochloride from PVA hydrogel embolic beads (DC Bead®, Biocompatibles UK Ltd, a BTG International group company) employed in chemoembolisation practice for treating hypervascularised tumours and arteriovenous malformations [67]. Specifically, here we evaluated the contribution of either the position/effectiveness of the embolic event and the hydrodynamic environment on the drug-elution process from single bead. For this purpose, we identified two distinct single-bead embolisation modes, classified as (i) *partially-confined embolisation*, in which bead is not fully penetrated within the embolised channel as a result of an

abrupt reduction of channel diameter at branching sites; and (ii) *completely-confined embolisation*, in which bead is fully penetrated within the embolised channel and displays a highly deformed shape.

Our experimental observations suggest that the two embolisation modes can have different implications in embolisation therapy, as initially hypothesised. Specifically, partially-confined embolisation of the channel resulted in faster drug-elution and in drug-elution kinetics being strongly influenced by the Reynolds number (and thus the mean fluid velocity) in the feeding channel. A non-intuitive dependence of drug-elution on the Reynolds number was identified, which was attributed to a bead dynamically changing its mechanical properties as a result of drug-elution, thus gradually penetrating into the embolised channel. This effect was particularly enhanced at the higher Re_{in}. Furthermore, partial bead exposure to the systemic fluid flow may have potentially caused less-targeted distribution of the eluted drug (see Supplementary Figure 4.1). Conversely, completely-confined embolisation resulted in a slow and sustained drug-elution, and in the elution dynamics being less influenced by the Reynolds number in the feeding channel. Also, we observed that effective completely-confined embolisation caused the onset of a peculiar fluid dynamic field in close proximity to the bead (i.e., laminar vortices, see Video 2), which is coherent with previous studies [37] and likely contributed to faster drug-elution from the bead surface area oriented towards the systemic circulation. This effect may potentially cause less-targeted elution and its minimisation may be desired. We are currently working on a better understanding of this mechanism.

To conclude, simplicity, reliability and the possibility to explore wide range of physiological conditions, make this technology suitable for the investigation of drug-elution kinetics from DEBs and screening of beads with different properties without resorting to labour-intensive processing.

5. Limitations

Limitations associated with the present study have been outlined in sub-paragraphs, as follows.

5.1 Optical system and fluorescence intensity calibration

From the recently published work of M. Biondi *et al.* [68], we could expect that at the doxorubicin concentration employed in this study quenching of the fluorescence signal would occur. When we examined single beads under fluorescence using our experimental set-up, we observed that the beads displayed a very intense fluorescence even upon a short exposure time (100 ms). We monitored fluorescence over time and found in all cases it diminished consistently, and at no point did we observe any increase in fluorescence that we might expect as the concentration dropped below that where quenching would no longer be occurring. We compared the fluorescence intensity with a calibration curve obtained using free drug in solution which we are aware may under-estimate the actual concentration but allows us to mathematically treat the data and then express it as fractional release rather than absolute amounts. We suspect this maybe a phenomenon due to the doxorubicin self-association inside the beads or other dilution effect of the drug released at the bead surface. Furthermore, it is proposed that the content of doxorubicin present in the test system would be significantly lower than the loaded 37.5 mg/mL. This estimate of the total drug volume can be calculated from a range encompassing a packed bead volume (77.83%) for which there is a known chemical volume of binding material for drug loading at 44.4% [69, 70]. This yields the total number of beads containing the 37.5 mg dose as approximately 27,000, with a single bead containing 1.39 μg assuming homogenous loading, which may explain the absence of quenching phenomena in our system.

We acknowledge the unclear nature of how fluorescence correlates to concentration within our system, and this will represent the subject of future investigations.

Additionally, the high depth of focus of our optical system allowed for capturing the fluorescence signal originating from a large portion of the bead. It is however likely that the on-chip method was not capable of detecting the total drug content.

5.2 Physical properties of the microfluidic environment

In the current generation of microfluidic devices, microchannel architecture reproduced key features of tumour microvascular systems. Notably, it was characterised by spatial asymmetry and presented a severe reduction of channel diameter from the proximal to the distal regions, coherently with uterine animal models [71]. Channels diameter fell into the range of small arteries and arterioles, which correspond to the vascular domain targeted by embolic particles. Notably, it was comparable with animal models employed in previous embolisation studies (i.e. animal kidney and uterus models) [72, 73].

Despite these geometrical similarities, the current microfluidic model does not faithfully mimic the physical properties of the physiological microenvironment. These include vessel distensibility and vessel wall permeability to bioactive molecules, both of which likely contribute to influence the kinetics of drug-elution *in vivo* [5]. Moreover, the effects of blood were not investigated, particularly the role of red blood cells on residual flow post embolisation when blood coagulation would occur. Also, fluid temperature and gas composition did not replicate those of physiological microenvironments. We are currently working on the development of a second generation of microfluidic devices which will also mimic these physical properties of microvascular systems.

5.3 Method validation

To conclude, a quantitative validation of our model with existing elution techniques is limited by the lack of single-bead elution methods. Notably, it is unlikely that there would be single beads

occluding vessels, more likely a chain of beads in which our elution studies here might represent effects on the terminal bead in the chain. The presence of multiple beads within the microchannel network system may have affected both the local fluid dynamic field (i.e., mean fluid velocity) and local drug concentration, thus influencing the kinetics of the drug elution process and the amount of eluted drug.

We however anticipate that, given the clinical relevance of single-bead embolisation processes [11], this will be a future avenue of research in the field of chemo-embolisation.

Videos

Video 1. Representative temporal evolution of the fluorescence intensity from a single, completely confined bead within the microfluidic device. Reduction of fluorescence intensity over time can be appreciated, which is particularly enhanced in the bead area exposed to laminar vortices.

Video 2. Representative flow visualisation experiment (using fluorescently labelled microbeads), showing the formation of a vortex within the cavity formed by a single bead (i.e., completely-confined) occluding a microchannel at a branching site.

Acknowledgment

Authors sincerely thank Biocompatibles UK Ltd (a BTG International group company) for providing embolic beads. This document is an output partially from the UKIERI (UK-India Education and Research Initiative) program (Project Code: SA08-086) funded by Department of Business, Innovation and Skills (BIS), Foreign and Commonwealth Office (FCO), British Council, Welsh Assembly Government and the Ministry of Human Resource Development (MHRD), Government of India.

Conflict of Interest

Marcus Caine and Andrew L Lewis are employees at Biocompatibles Ltd. (a BTG International group company) and they are working on the development of embolic devices, although they were not directly paid by the research project described in this study.

References

[1] J. Lemieux, E. Maunsell, L. Provencher, Chemotherapy-induced alopecia and effects on quality of life among women with breast cancer: a literature review, Psycho-Oncology, 17 (2008) 317-328.
[2] J.-J. Monsuez, J.-C. Charniot, N. Vignat, J.-Y. Artigou, Cardiac side-effects of cancer chemotherapy, International journal of cardiology, 144 (2010) 3-15.
[3] K. Hong, A. Khwaja, E. Liapi, M.S. Torbenson, C.S. Georgiades, J.-F.H. Geschwind, New intra-arterial drug delivery system for the treatment of liver cancer: preclinical assessment in a rabbit model of liver cancer, Clinical Cancer Research, 12 (2006) 2563-2567.
[4] M. Varela, M.I. Real, M. Burrel, A. Forner, M. Sala, M. Brunet, C. Ayuso, L. Castells, X. Montañá, J.M. Llovet, Chemoembolization of hepatocellular carcinoma with drug eluting beads: efficacy and doxorubicin pharmacokinetics, Journal of hepatology, 46 (2007) 474-481.
[5] A.L. Lewis, M.R. Dreher, Locoregional drug delivery using image-guided intra-arterial drug eluting bead therapy, Journal of Controlled Release, 161 (2012) 338-350.
[6] J. Bruix, M. Sala, J.M. Llovet, Chemoembolization for hepatocellular carcinoma, Gastroenterology, 127 (2004) S179-S188.
[7] R.R. Taylor, Y. Tang, M. Gonzalez, P.W. Stratford, A.L. Lewis, Irinotecan drug eluting beads for use in chemoembolization: In vitro and in vivo evaluation of drug release properties, European journal of pharmaceutical sciences, 30 (2007) 7-14.
[8] A. Nicolini, S. Crespi, L. Martinetti, Drug delivery embolization systems: a physician's perspective, Expert Opinion on Drug Delivery, 8 (2011) 1071-1084.
[9] E.K. Lang, Reduced systemic toxicity from superselective chemoembolization compared with systemic chemotherapy in patients with high-risk metastatic gestational trophoblastic disease, Cardiovascular and interventional radiology, 20 (1997) 280-284.

[10] J. Kettenbach, A. Stadler, I. Katzler, R. Schernthaner, M. Blum, J. Lammer, T. Rand, Drug-loaded microspheres for the treatment of liver cancer: review of current results, Cardiovascular and interventional radiology, 31 (2008) 468-476.
[11] J. Namur, S.J. Citron, M.T. Sellers, M.H. Dupuis, M. Wassef, M. Manfait, A. Laurent, Embolization of hepatocellular carcinoma with drug-eluting beads: doxorubicin tissue concentration and distribution in patient liver explants, Journal of hepatology, 55 (2011) 1332-1338.
[12] S. Vinchon-Petit, D. Jarnet, S. Michalak, A. Lewis, J.P. Benoit, P. Menei, Local implantation of doxorubicin drug eluting beads in rat glioma, International journal of pharmaceutics, 402 (2010) 184-189.
[13] M.A. Maluccio, A.M. Covey, L.B. Porat, J. Schubert, L.A. Brody, C.T. Sofocleous, G.I. Getrajdman, W. Jarnagin, R. DeMatteo, L.H. Blumgart, Transcatheter arterial embolization with only particles for the treatment of unresectable hepatocellular carcinoma, Journal of Vascular and Interventional Radiology, 19 (2008) 862-869.
[14] M. Burrel, M. Reig, A. Forner, M. Barrufet, C.R. Lope, S. Tremosini, C. Ayuso, J.M. Llovet, M.I. Real, J. Bruix, Survival of patients with hepatocellular carcinoma treated by transarterial chemoembolisation (TACE) using DC Beads. Implications for clinical practice and trial design, Journal of hepatology, 56 (2012) 1330-1335.
[15] E. Liapi, K.H. Lee, C.C. Georgiades, K. Hong, J.F.H. Geschwind, Drug-eluting particles for interventional pharmacology, Techniques in Vascular and Interventional Radiology, 10 (2007) 261-269.
[16] M. Varela, M.I. Real, M. Burrel, A. Forner, M. Sala, M. Brunet, C. Ayuso, L. Castells, X. Montaná, J.M. Llovet, Chemoembolization of hepatocellular carcinoma with drug eluting beads: efficacy and doxorubicin pharmacokinetics, Journal of hepatology, 46 (2007) 474-481.
[17] A.L. Lewis, M.V. Gonzalez, S.W. Leppard, J.E. Brown, P.W. Stratford, G.J. Phillips, A.W. Lloyd, Doxorubicin eluting beads - 1: Effects of drug loading on bead characteristics and drug distribution, Journal of Materials Science: Materials in Medicine, 18 (2007) 1691-1699.
[18] Y. Bayraktar, F. Balkanci, B. Kayhan, B. Uzunalimoglu, A. Gokoz, Y. Ozisik, A. Gurakar, D. Van Thiel, D. Firat, A comparison of chemoembolization with conventional chemotherapy and symptomatic treatment in cirrhotic patients with hepatocellular carcinoma, Hepato-gastroenterology, 43 (1996) 681-687.
[19] R.T.P. Poon, W.K. Tso, R.W.C. Pang, K.K.C. Ng, R. Woo, K.S. Tai, S.T. Fan, A phase I/II trial of chemoembolization for hepatocellular carcinoma using a novel intra-arterial drug-eluting bead, Clinical Gastroenterology and Hepatology, 5 (2007) 1100-1108.
[20] K. Malagari, M. Pomoni, H. Moschouris, E. Bouma, J. Koskinas, A. Stefaniotou, A. Marinis, A. Kelekis, E. Alexopoulou, A. Chatziioannou, Chemoembolization with doxorubicin-eluting beads for unresectable

hepatocellular carcinoma: five-year survival analysis, Cardiovascular and interventional radiology, 35 (2012) 1119-1128.
[21] E. Liapi, C.C. Georgiades, K. Hong, J.F.H. Geschwind, Transcatheter arterial chemoembolization: current technique and future promise, Techniques in Vascular and Interventional Radiology, 10 (2007) 2-11.
[22] T. Livraghi, Radiofrequency ablation, PEIT, and TACE for hepatocellular carcinoma, Journal of hepato-biliary-pancreatic surgery, 10 (2003) 67-76.
[23] C. Cammà, F. Schepis, A. Orlando, M. Albanese, L. Shahied, F. Trevisani, P. Andreone, A. Craxì, M. Cottone, Transarterial Chemoembolization for Unresectable Hepatocellular Carcinoma: Meta-Analysis of Randomized Controlled Trials1, Radiology, 224 (2002) 47-54.
[24] S.P. Kalva, M. Pectasides, R. Liu, N. Rachamreddy, S. Surakanti, K. Yeddula, S. Ganguli, S. Wicky, L.S. Blaszkowsky, A.X. Zhu, Safety and effectiveness of chemoembolization with drug-eluting beads for advanced-stage hepatocellular carcinoma, Cardiovascular and interventional radiology, 37 (2014) 381-387.
[25] R. Golfieri, E. Giampalma, M. Renzulli, R. Cioni, I. Bargellini, C. Bartolozzi, A. Breatta, G. Gandini, R. Nani, D. Gasparini, Randomised controlled trial of doxorubicin-eluting beads vs conventional chemoembolisation for hepatocellular carcinoma, British journal of cancer, 111 (2014) 255-264.
[26] V. Anand, R. Kandarapu, S. Garg, Ion-exchange resins: carrying drug delivery forward, Drug discovery today, 6 (2001) 905-914.
[27] A.L. Lewis, M. Gonzalez, A.W. Lloyd, B. Hall, Y. Tang, S.L. Willis, S.W. Leppard, L.C. Wolfenden, R.R. Palmer, P.W. Stratford, DC bead: in vitro characterization of a drug-delivery device for transarterial chemoembolization, Journal of Vascular and Interventional Radiology, 17 (2006) 335-342.
[28] M.V. Gonzalez, Y. Tang, G.J. Phillips, A.W. Lloyd, B. Hall, P.W. Stratford, A.L. Lewis, Doxorubicin eluting beads - 2: methods for evaluating drug elution and in-vitro:in-vivo correlation, Journal of Materials Science: Materials in Medicine, 19 (2008) 767-775.
[29] P.J. Dowding, B. Vincent, Suspension polymerisation to form polymer beads, Colloids and Surfaces A: Physicochemical and Engineering Aspects, 161 (2000) 259-269.
[30] M. Lubarsky, C.E. Ray Jr, B. Funaki, Embolization Agents - Which One Should Be Used When? Part 1: Large-Vessel Embolization, in, Thieme Medical Publishers, 2009, pp. 352.
[31] M. Lubarsky, C. Ray, B. Funaki, Embolization Agents - Which One Should Be Used When? Part 2: Small-Vessel Embolization, in, Thieme Medical Publishers, 2010, pp. 99.
[32] A. Lewis, C. Adams, W. Busby, S. Jones, L. Wolfenden, S. Leppard, R. Palmer, S. Small, Comparative in vitro evaluation of microspherical embolisation agents, Journal of Materials Science: Materials in Medicine, 17 (2006) 1193-1204.

[33] T. Das, D. Carugo, X. Zhang, S. Chakraborty, Oscillation dynamics of embolic microspheres in flows with red blood cell suspensions, Journal of Applied Physics, 112 (2012) 1-7.
[34] D. Carugo, L. Capretto, S. Willis, A.L. Lewis, D. Grey, M. Hill, X. Zhang, A microfluidic device for the characterisation of embolisation with polyvinyl alcohol beads through biomimetic bifurcations, Biomedical microdevices, 14 (2011) 153-163.
[35] C. Senturk, V. Cakir, K. Yorukoglu, O. Yilmaz, A.Y. Goktay, Looking for the ideal particle: an experimental embolization study, Cardiovascular and interventional radiology, 33 (2010) 336-345.
[36] R. López-Benítez, G.M. Richter, H.U. Kauczor, S. Stampfl, J. Kladeck, B.A. Radeleff, M. Neukamm, P.J. Hallscheidt, Analysis of nontarget embolization mechanisms during embolization and chemoembolization procedures, Cardiovascular and interventional radiology, 32 (2009) 615-622.
[37] F. Amyot, K. Jurski, J. Dufaux, G. Guiffant, An experimental and theoretical study of mass transfer from loaded embolisation microbeads: possible optimisation, International communications in heat and mass transfer, 29 (2002) 623-632.
[38] K. Fuchs, P.E. Bize, A. Denys, G. Borchard, O. Jordan, Sunitinib-eluting beads for chemoembolization: Methods for in vitro evaluation of drug release, International journal of pharmaceutics, 482 (2015) 68-74.
[39] S. McDougall, A. Anderson, M. Chaplain, J. Sherratt, Mathematical modelling of flow through vascular networks: Implications for tumour-induced angiogenesis and chemotherapy strategies, Bulletin of Mathematical Biology, 64 (2002) 673-702.
[40] L. Capretto, W. Cheng, D. Carugo, O.L. Katsamenis, M. Hill, X. Zhang, Mechanism of co-nanoprecipitation of organic actives and block copolymers in a microfluidic environment, Nanotechnology, 23 (2012) 375602-375616.
[41] D. Carugo, D.N. Ankrett, P. Glynne-Jones, L. Capretto, R.J. Boltryk, X. Zhang, P.A. Townsend, M. Hill, Contrast agent-free sonoporation: The use of an ultrasonic standing wave microfluidic system for the delivery of pharmaceutical agents, Biomicrofluidics, 5 (2011) 044108-044115.
[42] B. Roy, T. Das, T.K. Maiti, S. Chakraborty, Effect of fluidic transport on the reaction kinetics in lectin microarrays, Analytica chimica acta, 701 (2011) 6-14.
[43] D. Carugo, L. Capretto, E. Nehru, M. Mansour, N. Smyth, N. Bressloff, X. Zhang, A Microfluidic-Based Arteriolar Network Model for Biophysical and Bioanalytical Investigations, Current Analytical Chemistry, 9 (2013) 47-59.
[44] A. Laurent, M. Wassef, J. Namur, H. Ghegediban, J. Pelage, Arterial distribution of calibrated tris-acryl gelatin and polyvinyl alcohol embolization microspheres in sheep uterus, Cardiovascular and interventional radiology, 33 (2010) 995-1000.
[45] G.M. Tozer, S.M. Ameer-Beg, J. Baker, P.R. Barber, S.A. Hill, R.J. Hodgkiss, R. Locke, V.E. Prise, I. Wilson, B. Vojnovic, Intravital imaging of tumour vascular

networks using multi-photon fluorescence microscopy, Advanced drug delivery reviews, 57 (2005) 135-152.
[46] D.N. Ku, Blood flow in arteries, Annual Review of Fluid Mechanics, 29 (1997) 399-434.
[47] A. Tailor, D. Jurkovic, T.H. Bourne, M. Natucci, W.P. Collins, S. Campbell, A comparison of intratumoural indices of blood flow velocity and impedance for the diagnosis of ovarian cancer, Ultrasound in medicine & biology, 22 (1996) 837-843.
[48] K. Shimamoto, S. Sakuma, T. Ishigaki, N. Makino, Intratumoral blood flow: evaluation with color Doppler echography, Radiology, 165 (1987) 683-685.
[49] R.K. Jain, Determinants of tumor blood flow: a review, Cancer research, 48 (1988) 2641-2658.
[50] D. Fukumura, D.G. Duda, L.L. Munn, R.K. Jain, Tumor Microvasculature and Microenvironment: Novel Insights Through Intravital Imaging in Pre-Clinical Models, Microcirculation, 17 (2010) 206-225.
[51] H. Zhang, F. Li, J. Yi, C. Gu, L. Fan, Y. Qiao, C. Cheng, H. Wu, Folate-decorated maleilated pullulan-doxorubicin Conjugate for active tumor-targeted drug delivery, European journal of pharmaceutical sciences, 42 (2011) 517-526.
[52] G. Hempel, P. Schulze-Westhoff, S. Flege, N. Laubrock, J. Boos, Therapeutic drug monitoring of doxorubicin in paediatric oncology using capillary electrophoresis, Electrophoresis, 19 (1998) 2939-2943.
[53] F. Ungaro, M. Biondi, I. d'Angelo, L. Indolfi, F. Quaglia, P.A. Netti, M.I. La Rotonda, Microsphere-integrated collagen scaffolds for tissue engineering: effect of microsphere formulation and scaffold properties on protein release kinetics, Journal of controlled release, 113 (2006) 128-136.
[54] M. Biondi, L. Indolfi, F. Ungaro, F. Quaglia, M.I. La Rotonda, P.A. Netti, Bioactivated collagen-based scaffolds embedding protein-releasing biodegradable microspheres: tuning of protein release kinetics, Journal of Materials Science: Materials in Medicine, 20 (2009) 2117-2128.
[55] M.R. Dreher, K.V. Sharma, D.L. Woods, G. Reddy, Y. Tang, W.F. Pritchard, O.A. Chiesa, J.W. Karanian, J.A. Esparza, D. Donahue, Radiopaque Drug-Eluting Beads for Transcatheter Embolotherapy: Experimental Study of Drug Penetration and Coverage in Swine, Journal of Vascular and Interventional Radiology, 23 (2011) 257-264.
[56] Y.P. Gobin, F. Viñuela, H.V. Vinters, C. Ji, K. Chow, Embolization with Radiopaque Microbeads of Polyacrylonitrile Hydrogel: Evaluation in Swine1, Radiology, 214 (2000) 113-119.
[57] A. Laurent, E. Velzenberger, M. Wassef, J. Pelage, A. Lewis, Do microspheres with narrow or standard size distributions localize differently in vasculature? An experimental study in sheep kidney and uterus, Journal of Vascular and Interventional Radiology, 19 (2008) 1733-1739.

[58] E. Liapi, C. Georgiades, K. Hong, J. Geschwind, Transcatheter arterial chemoembolization: current technique and future promise, Techniques in Vascular and Interventional Radiology, 10 (2007) 2-11.
[59] J. Hamada, Y. Kai, S. Nagahiro, N. Hashimoto, H. Iwata, Y. Ushio, Embolization with cellulose porous beads, II: Clinical trial, American journal of neuroradiology, 17 (1996) 1901-1906.
[60] J. Hamada, Y. Ushio, K. Kazekawa, T. Tsukahara, N. Hashimoto, H. Iwata, Embolization with cellulose porous beads, I: An experimental study, American journal of neuroradiology, 17 (1996) 1895-1899.
[61] A. Laurent, M. Wassef, J. Saint Maurice, J. Namur, J. Pelage, A. Seron, R. Chapot, J. Merland, Arterial distribution of calibrated tris-acryl gelatin and polyvinyl alcohol microspheres in a sheep kidney model, Investigative radiology, 41 (2006) 8-14.
[62] J. Dion, R. Rankin, F. Vinuela, A. Fox, A. Wallace, M. Mervart, Dextran microsphere embolization: experimental and clinical experience with radiologic-pathologic correlation. Work in progress, Radiology, 160 (1986) 717-721.
[63] A.L. Lewis, R.R. Taylor, B. Hall, M. Gonzalez, S.L. Willis, P.W. Stratford, Pharmacokinetic and safety study of doxorubicin-eluting beads in a porcine model of hepatic arterial embolization, Journal of Vascular and Interventional Radiology, 17 (2006) 1335-1343.
[64] A.L. Lewis, R.R. Holden, DC Bead embolic drug-eluting bead: clinical application in the locoregional treatment of tumours, Expert opinion on drug delivery, 8 (2011) 153-169.
[65] J. Guermond, C. Migeon, G. Pineau, L. Quartapelle, Start-up flows in a three-dimensional rectangular driven cavity of aspect ratio 1: 1: 2 at Re = 1000, Journal of Fluid Mechanics, 450 (2002) 169-200.
[66] C.J. Freitas, R.L. Street, A.N. Findikakis, J.R. Koseff, Numerical simulation of three-dimensional flow in a cavity, International journal for numerical methods in fluids, 5 (1985) 561-575.
[67] K. Malagari, E. Emmanouil, M. Pomoni, D. Kelekis, Chemoembolization with DC Bead™ for the treatment of hepatocellular carcinoma: an update, Hepatic Oncology, 1 (2014) 205-214.
[68] M. Biondi, S. Fusco, A.L. Lewis, P.A. Netti, New insights into the mechanisms of the interactions between doxorubicin and the ion-exchange hydrogel DC Bead™ for use in transarterial chemoembolization (TACE), Journal of Biomaterials Science, Polymer Edition, 23 (2012) 333-354.
[69] M.V. Gonzalez, Y. Tang, G.J. Phillips, A.W. Lloyd, B. Hall, P.W. Stratford, A.L. Lewis, Doxorubicin eluting beads—2: methods for evaluating drug elution and in-vitro: in-vivo correlation, Journal of Materials Science: Materials in Medicine, 19 (2008) 767-775.
[70] A.L. Lewis, M.V. Gonzalez, S.W. Leppard, J.E. Brown, P.W. Stratford, G.J. Phillips, A.W. Lloyd, Doxorubicin eluting beads− 1: Effects of drug loading on

bead characteristics and drug distribution, Journal of Materials Science: Materials in Medicine, 18 (2007) 1691-1699.
[71] A. Laurent, M. Wassef, J. Namur, H. Ghegediban, J.-P. Pelage, Arterial distribution of calibrated tris-acryl gelatin and polyvinyl alcohol embolization microspheres in sheep uterus, Cardiovascular and interventional radiology, 33 (2010) 995-1000.
[72] E. de Luis, J.I. Bilbao, J.A.G.J. de Ciércoles, A. Martínez-Cuesta, A. de Martino Rodríguez, M.D. Lozano, In vivo evaluation of a new embolic spherical particle (HepaSphere) in a kidney animal model, Cardiovascular and interventional radiology, 31 (2008) 367-376.
[73] A. Laurent, E. Velzenberger, M. Wassef, J.-P. Pelage, A.L. Lewis, Do microspheres with narrow or standard size distributions localize differently in vasculature? An experimental study in sheep kidney and uterus, Journal of Vascular and Interventional Radiology, 19 (2008) 1733-1739.

Graphical abstract